In vivo multiphoton fluorescence lifetime imaging of protein-bound and free nicotinamide adenine dinucleotide in normal and precancerous epithelia

Melissa C. Skala
Duke University
Department of Biomedical Engineering
Durham, North Carolina 27708

Kristin M. Riching
University of Wisconsin
Department of Biomedical Engineering
Madison, Wisconsin 53706

Damian K. Bird*
University of Wisconsin
Laboratory for Optical and Computational Instrumentation
Madison, Wisconsin 53706

Annette Gendron-Fitzpatrick
University of Wisconsin
Research Animal Resources Center
Madison, Wisconsin 53706

Jens Eickhoff
University of Wisconsin
Department of Biostatistics and Medical Informatics
Madison, Wisconsin 53706

Kevin W. Eliceiri
University of Wisconsin
Laboratory for Optical and Computational Instrumentation
Madison, Wisconsin 53706

Patricia J. Keely
University of Wisconsin
Department of Pharmacology
Madison, Wisconsin 53706

Nirmala Ramanujam
Duke University
Department of Biomedical Engineering
Durham, North Carolina 27708

Abstract. Multiphoton fluorescence lifetime imaging microscopy (FLIM) is a noninvasive, cellular resolution, 3-D functional imaging technique. We investigate the potential for *in vivo* precancer diagnosis with metabolic imaging via multiphoton FLIM of the endogenous metabolic cofactor nicotinamide adenine dinucleotide (NADH). The dimethylbenz[α]anthracene (DMBA)-treated hamster cheek pouch model of oral carcinogenesis and MCF10A cell monolayers are imaged using multiphoton FLIM at 780-nm excitation. The cytoplasm of normal hamster cheek pouch epithelial cells has short (0.29 ± 0.03 ns) and long lifetime components (2.03 ± 0.06 ns), attributed to free and protein-bound NADH, respectively. Low-grade precancers (mild to moderate dysplasia) and high-grade precancers (severe dysplasia and carcinoma *in situ*) are discriminated from normal tissues by their decreased protein-bound NADH lifetime ($p < 0.05$). Inhibition of cellular glycolysis and oxidative phosphorylation in cell monolayers produces an increase and decrease, respectively, in the protein-bound NADH lifetime ($p < 0.05$). Results indicate that the decrease in protein-bound NADH lifetime with dysplasia is due to a shift from oxidative phosphorylation to glycolysis, consistent with the predictions of neoplastic metabolism. We demonstrate that multiphoton FLIM is a powerful tool for the noninvasive characterization and detection of epithelial precancers *in vivo*. [DOI: 10.1117/1.2717503]

Keywords: metabolism; oral cancer; multiphoton microscopy; animal model.

Paper 06190R received Jul. 21, 2006; revised manuscript received Oct. 23, 2006; accepted for publication Nov. 28, 2006; published online Apr. 10, 2007.

1 Introduction

Fluorescence lifetime imaging microscopy (FLIM) is a functional imaging technique that probes the excited state lifetime of a fluorophore. The excited state lifetime can be altered by the fluorophore microenvironment, including factors such as local pH, temperature, viscosity, and oxygen concentration.[1] FLIM, which relies on the temporally resolved fluorescence signal, is advantageous over fluorescence intensity or spectral measurements for small-volume tissue imaging because it is

*Current Affiliation: University of Melbourne, Photophysics and Photochemistry Group, Victoria 3010, Australia.
Address all correspondence to: Nirmala Ramanujam, Duke University, Department of Biomedical Engineering, Room 2575 CIEMAS, Durham, North Carolina 27708-0281; Tel: 919–660–5307; Fax: 919–684–4488; E-mail: nimmi@duke.edu

1083-3668/2007/12(2)/024014/10/$25.00 © 2007 SPIE

independent of fluorophore concentration, and minimally affected by tissue absorption and scattering, and fluctuations in excitation intensity.[2] Multiphoton-excited FLIM can generate 3-D images of fluorophore lifetimes with cellular and subcellular resolution.[1] The near-infrared (NIR) excitation used in multiphoton microscopy[3] enables greater penetration depths[4] and improved tissue viability[5] compared to single-photon excitation. An intuitive application of multiphoton FLIM is to exploit the endogenous fluorescence contrast from electron carriers, reduced nicotinamide adenine dinucleotide (NADH) and flavin adenine dinucleotide (FAD) already present in tissue for the early detection of cancer.

One of the hallmarks of carcinogenesis is a shift from cellular oxidative phosphorylation to cellular glycolysis for ATP production (the Warburg effect[6,7]). The endogenous fluorophore NADH is the principal electron acceptor in glycolysis and electron donor in oxidative energy metabolism. NADH has a short and long lifetime component, respectively, depending on whether it is in a free or protein-bound state.[8] The short lifetime of NADH in its free state is due to dynamic quenching by the adenine moiety.[2] Many enzymes bind to NADH in the metabolic pathway,[9] and as favored metabolic pathways shift with cancer progression, the distribution of NADH binding sites change.[10] The fluorescence lifetime of protein-bound NADH changes depending on the enzyme it is bound to.[11] This suggests that changes in metabolism with cancer development can be probed by the lifetime of protein-bound NADH.

The goal of our work was to exploit multiphoton FLIM of protein-bound NADH for metabolic imaging of epithelial precancers *in vivo*. To our knowledge, this is the first study to image changes in the lifetime of protein-bound NADH and relative abundance of free and protein-bound NADH with neoplastic progression *in vivo*. The study described in this paper consists of two parts. In the first part of the study, changes in the lifetime of protein-bound NADH and relative abundance of free and protein-bound NADH with inhibition of specific metabolic pathways were quantified. Specifically, multiphoton FLIM was carried out on an MCF10A cell culture model before and after inhibition with 3-bromopyruvate or cobalt chloride ($CoCl_2$). Glycolysis was inhibited with 3-bromopyruvate, which inhibits glyceraldehyde-3-phosphate dehydrogenase and 3-phosphoglycerate kinase in a competitive manner.[12,13] Oxidative phosphorylation was inhibited with $CoCl_2$, which mimics hypoxia by increasing the generation of reactive oxygen species during normoxia; upregulating hypoxia-inducible factor-1α, erythropoietin, and glycolytic enzymes.[14,15] $CoCl_2$ and 3-bromopyruvate produced a decrease and increase, respectively, in the lifetime of protein-bound NADH, and both perturbations produced a decrease in the abundance of protein-bound NADH relative to free NADH. The results of these characterization studies suggest that protein-bound NADH fluorescence lifetimes would be particularly sensitive to changes in glycolysis and/or oxidative phosphorylation.

In the second part of the study, multiphoton FLIM was used to investigate the lifetime of protein-bound NADH and the relative abundance of free and protein-bound NADH in normal and dysplastic tissues in the dimethylbenz [α]anthracene (DMBA)-treated hamster cheek pouch model of carcinogenesis at 780-nm excitation. The DMBA-treated hamster cheek pouch model was selected for this study because it has been shown to mimic the dysplasia-carcinoma sequence in the human oral cavity[16–18] and different stages of dysplasia and carcinoma can be examined over a relatively short period of time. The results of this study indicate that the protein-bound NADH lifetime decreases with low-grade precancers (mild to moderate dysplasia) and high-grade precancers [severe dysplasia and carcinoma *in situ* (CIS)] compared to normal tissues, and the abundance of protein-bound NADH relative to free NADH decreases with low-grade precancers *in vivo*.

2 Materials and Methods

2.1 *Imaging Instrumentation*

Two separate-custom designed multiphoton time-domain lifetime systems were employed at the University of Wisconsin for the cell culture and *in vivo* experiments. The system used for cell culture experiments was constructed[19] around a Nikon Eclipse TE300. A titanium-sapphire laser (Spectra-Physics-Millennium/Tsunami, 82 MHz, 100 fs) pumped by a 5-W Millenia was used as an excitation source at 780-nm excitation for FLIM, and at both 780- and 890-nm excitation for intensity redox imaging. Other components include a Nikon 40× Plan Apo oil-immersion lens [numerical aperture (NA)=1.3], and a dichromatic mirror (BG39, Schott, Elmsford, New York) that enabled the 780-nm excitation light to reflect onto the sample and wavelengths between 400 and 600 nm to transmit to the detector. Intensity and FLIM data were collected pixel by pixel by a laser scanning unit (based on a BioRad, MRC-600) and a GaAsP photon-counting photomultiplier tube (PMT) (H7422, Hamamatsu) connected to a time-correlated single-photon counting (TCSPC) system (SPC-730, Becker & Hickl).

All *in vivo* multiphoton FLIM images were collected with a second system constructed around a Nikon Diaphot 200 microscope.[20] The excitation source is a titanium-sapphire laser (Coherent, Mira; 76 MHz, 120 fs) pumped by an 8-W solid state laser (Coherent, Verdi). Other components include a 60× oil-immersion objective (Nikon, PlanApo NA=1.4), and a dichromatic mirror (650DCSP, Chroma Technology, Rockingham, Vermont) to reflect the 780-nm excitation light onto the sample and transmit wavelengths between 400 and 650 nm to the detector. FLIM data were collected pixel by pixel with a laser scanning unit (BioRad, MRC-600), a fast photon-counting PMT (Becker & Hickl, PMH-100), and TCSPC electronics (Becker & Hickl, SPC-830). To control the power coupled to the system, a variable neutral density filter wheel was positioned before the entrance to the scanning unit. Acquisition for both systems was done with WiscScan,[21] a lab-developed software package.

2.2 *Cell Culture Perturbation Experiments*

MCF10A cells were obtained from the American Type Culture Collection.[22] The cells remained free of mycoplasma and other contaminants and were propagated by adherent culture according to established protocols.[23] MCF10A cells were grown in DMEM-F12 supplemented with 5% horse serum, 20-ng/mL epidermal growth factor, 10-μg/mL insulin, and 0.5-mg/mL hydrocortisone. Plated cells were stored in a 10%

CO_2 incubator at 37°C and cultured every 3 to 4 days. Cells were detached from the flasks by trypsinization and triply washed in 10 mL of phospate-buffered saline (PBS). A hemacytometer was used to determine the concentration of the cells by counting the number of cells per milliliter. On determination of the concentration of the cells, the volumes required to plate 25,000 and 1,000,000 cells per dish were calculated, respectively. MCF10A cells at the two different densities were plated on lysine-coated cover-glass-bottom Petri dishes (size, 35 mm; P35G-0-41-C, MatTek, Ashland, Massachusetts) and immersed in their standard growth media. Two different cell concentrations were used for these experiments because previous work has shown that the lifetime of NADH in cell culture depends on the cell confluency (due to changes in metabolism with cell confluency).[24]

Redox ratio images,[25] which are defined as the fluorescence intensity of FAD divided by the sum of the fluorescence intensities of FAD and NADH, can be used to measure relative changes in the oxidation-reduction state of cells. Redox ratio imaging was used to verify that the concentrations and incubation times of 3-bromopyruvate- and $CoCl_2$-produced changes in cellular metabolism. Cells were either left untreated (control), treated with 300-μM 3-bromopyruvate (Sigma-Aldrich, St. Louis, Missouri) for 60 to 90 min to inhibit glycolysis, or treated with 200-μM $CoCl_2$ (Sigma-Aldrich, St. Louis, Missouri) for 60 to 90 min to inhibit oxidative phosphorylation, as verified by changes in the redox ratio. NADH lifetime and intensity images were collected at a two-photon excitation wavelength of 780 nm and FAD intensity images were collected at 890-nm excitation.[26] At the completion of the final image acquisition, cell viability was confirmed under light microscopy (using the same microscope) by trypan blue exclusion. All cell dishes remained viable throughout any given imaging session.

The average power for the cell imaging experiments was approximately 15 mW, and the scan area for each image plane was 256×256 pixels (165×165 μm). Single-photon counting was done at a rate of approximately 500×10^5 photons/s for a total of 60 s with a pixel dwell time of approximately 11.5 μs (i.e., 11.5 μs dwell time on each of 256×256 pixels). Thus, over ~80 frames were averaged to generate each image. Photon count rates at the beginning and end of image acquisition were monitored to ensure that photobleaching did not occur. The instrument response function (IRF) was measured using a second-harmonic-generated signal from a β-BaB_2O_4 crystal.[20] The full width at half maximum (FWHM) of the IRF was 0.313 ns for the cell culture experiments. This represents the IRF of the overall system where the components that mainly contribute to temporal degradation are the transient time spread of the detector, optical dispersion at mirrors and through lenses, and light scattering at diaphragms.

2.3 *DMBA-Treated Hamster Cheek Pouch Model of Oral Cancer*

A total of 13 DMBA-treated and 9 control male Golden Syrian hamsters were evaluated in this study (average weight: 156±13 g). Animal care and procedures were in accordance with the guidelines in the U.S. Department of Health and Human Services and National Institutes of Health "Guide for the Care and Use of Laboratory Animals" and approved by the Institutional Animal Care and Use Committee at the University of Wisconsin. For each hamster, the right cheek pouch was either treated three times per week with 0.5% DMBA (by weight, Sigma-Aldrich, St. Louis, Missouri) in mineral oil (DMBA-treated animals), or the right cheek pouch was treated at the same frequency with mineral oil only (control animals) for a total of 16 weeks. The treatment schedule and procedures were established from previous studies.[27,28] At 16 to 21 weeks after the commencement of DMBA or mineral oil treatment, the cheek pouch of each animal was imaged using multiphoton FLIM at an excitation wavelength of 780 nm, which falls within the absorption band[26] of NADH. This wavelength was also selected because statistically significant differences in tissue fluorescence intensity have been observed[28] between normal tissues, dysplasias, and carcinomas in the hamster cheek pouch model with multiphoton microscopy at a two-photon excitation wavelength of 780 nm.

Prior to imaging, each hamster was anesthetized with an intraperitoneal injection of a mixture of 2.5 mg/kg acepromazine, 200 mg/kg ketamine, and 5 mg/kg xylazine. Next, the cheek pouch was inverted and stretched over an 8-mm-diam cork, pinned to the sides of the cork with two 27-gauge needles, and then wiped with saline. A cover slip was secured on the objective side of a 10-mm-diam opening in the imaging stage using Vaseline. The animal was placed on its stomach, and the cork was secured to the imaging stage of the inverted microscope such that the cheek was flush against the cover slip. The microscope objective was centered within the 10-mm opening of the imaging stage prior to image collection.

The average power incident on the sample ranged from approximately 3.3 to 7.2 mW. Single-photon counting was done at a rate of approximately 500×10^5 photons/s for 45 s to 5 min with a pixel dwell time of approximately 6.25 μs. The scan area at each image plane was 256×256 pixels (140×140 μm). Photon count rates at the beginning and end of image acquisition were monitored to ensure that photobleaching did not occur. The image z stacks were generated using a 10-μm z step size.

To ensure instrument consistency between experimental days, the lifetime of a known and stable instrument standard, 20-μm-diam Fluoresbrite YG (yellow green) microspheres (Polysciences Inc.) was imaged at the beginning of each day of the *in vivo* experiments ($n=14$). The microspheres were measured under the same experimental conditions as the *in vivo* measurements, except the power at the sample and the integration time were adjusted to achieve a single photon count rate of approximately 500×10^5 from the significantly brighter microspheres. The lifetime decay curves measured from the microspheres were fit to a single exponential decay model using SPCImage software (see later). The average lifetime for the microspheres ($n=14$) was 2.13±0.11 ns. The measured value for the lifetime of these spheres is consistent with that reported in other studies[24,29] (~2.2±0.1 ns). The IRF measured using a second-harmonic-generated signal from a β-BaB_2O_4 crystal had an FWHM of 0.190±0.002 ns for the *in vivo* experiments. The IRF for the *in vivo* experiments differs from that of the cell culture experiments due to differ-

ent detectors and optical paths in the two multiphoton FLIM systems.

After *in vivo* imaging, a biopsy was taken from the imaged site (center of the 10-mm stage opening) with a 3-mm-diam dermal biopsy punch. The biopsy was placed in 10% buffered formalin and submitted for histopathology. The tissue biopsies were cut and stained with hematoxylin and eosin (H&E), and read by a board certified veterinary pathologist (Annette Gendron-Fitzpatrick). Diagnosis was based on established criteria,[30] with tissues assigned to one of the following categories: normal, hyperplasia, mild dysplasia, moderate dysplasia, severe dysplasia, papillary hyperplasia/papilloma, CIS, or squamous cell carcinoma (SCC). The diagnosis for a given biopsy was determined from an evaluation of multiple sections cut from that biopsy. If any of these tissue biopsies were found to have more than one diagnosis (for example, severe dysplasia and SCC), the most severe diagnosis was assigned to that biopsy. FLIM images were taken from a microscopic field of view (140×140 μm), thus it was difficult to mark the precise image site on the biopsy. The approach taken in this study was to assign a diagnosis to each image stack based on the most severe pathologic diagnosis of the entire corresponding biopsy sample. This approach was consistent with that reported in our previous study, which employed multiphoton microscopy to characterize the NADH intensity in the hamster cheek pouch model of carcinogenesis.[28]

2.4 *Analysis of the Fluorescence Lifetime Decay Curves*

SPCImage software (Becker & Hickl) was used to analyze the fluorescence lifetime decay curves.[24] First, the measured lifetime decay curve was binned over the pixel of interest and the eight-nearest neighbor pixels. Each set of binned pixels was fit independently. Next, the measured instrument response was convolved with the model, and this reconvolved model was fit to the measured lifetime decay curve for a given set of binned pixels. This produced a lifetime decay curve with a peak value of approximately 100 counts. The lifetime decay curve of the pixel of interest was then fit to a double-exponential decay model:

$$F(t) = \alpha_1 \exp(-t/\tau_1) + \alpha_2 \exp(-t/\tau_2) + \mathbf{C},$$

where $F(t)$ is the fluorescence intensity at time t after the excitation light has ceased, τ_1 and τ_2 are the fluorophore lifetimes (τ_1 is the short-lifetime component and τ_2 is the long-lifetime component), and α_1 and α_2 are the relative contributions of the lifetime components (i.e., $\alpha_1 + \alpha_2 = 100\%$), and C is a constant pertaining to the level of background light present in most practical situations. The lifetime for the pixel of interest was calculated by finding the global minimum of the χ^2 value. The minimum calculated lifetime constrained by the fit model in SPCImage was 0.1 ns, which is close to the temporal response of the multiphoton FLIM system. The mean and standard deviation of the χ^2 value (a χ^2 value close to 1 indicates a good fit) for the entire field of view of all *in vivo* hamster cheek pouch images and *in vitro* cell culture image planes was 1.05 ± 0.05 and 1.01 ± 0.01, respectively. A survey of χ^2 values on a few samples indicated that the double-exponential decay model improved the χ^2 value of the fit over the single-exponential decay model, and the triple-exponential decay model did not improve the χ^2 value of the fit compared to the double-exponential decay model. The presence of two distinctly different lifetimes for free and protein-bound NADH (Refs. 8 and 31) also indicates that NADH fluorescence decay curves are best fit to a double-exponential decay model. Simulated fluorescence lifetime decay curves indicate that the τ_1, τ_2, α_1, and α_2 recovered with SPCImage from high-SNR decay curves are accurate to within 1%, and results achieved from simulated lifetime decay curves with an SNR similar to the measured *in vivo* and *in vitro* lifetime decay curves are accurate to within 6%.

2.5 *Quantification of Variables from the FLIM Images for Statistical Analyses*

2.5.1 *Cell culture*

All FLIM and fluorescence intensity images at a given cell density (low or high) were obtained on the same day (for a total of two experimental days, one for each of the two cell densities). For the analysis of cell culture lifetime images, the region of interest (ROI) containing the cells was selected, and the fluorescence intensity threshold in SPCImage was adjusted so that signals from the nucleus were below the threshold. The ROI included as few as 2 cells (low cell density) or as many as 60 cells (high cell density). Next, the lifetimes of all pixels in the ROI were calculated, and the mean value of τ_1, τ_2, and α_2 were recorded for each of the three ROIs per dish. The redox ratio [fluorescence intensity of FAD/(FAD +NADH)] was calculated from the mean intensity of the 890-nm excitation images (FAD) and the mean intensity of the corresponding 780-nm excitation images (NADH). The mean redox ratio was recorded for each of the three ROIs per dish. All redox ratio images at a given cell density were collected under identical experimental conditions on the same day. High-density cells included control cells ($n=8$ total ROIs from four dishes), cells treated with 3-bromopyruvate ($n=6$ total ROIs from two dishes), and cells treated with $CoCl_2$ ($n=6$ total ROIs from two dishes). Low-density cells included control cells ($n=5$ total ROIs from two dishes), cells treated with 3-bromopyruvate ($n=6$ total ROIs from two dishes), and cells treated with $CoCl_2$ ($n=6$ total ROIs from two dishes).

2.5.2 *Hamster cheek pouch model*

The epithelium and stroma were analyzed separately by choosing volumes of interest based on morphology. For the analysis of the epithelial layer, three cells were randomly chosen in each image plane within a depth stack of multiple image planes within an animal. The fluorescence intensity threshold in SPCImage was adjusted so that signals from the nucleus were below the threshold, and the lifetimes were calculated per pixel from all pixels within each cell. Separate matrices for τ_1, τ_2, and α_2 for each cell were exported to MATLAB (The Mathworks, Inc., Natick, Massachusetts). Then the mean and standard deviation of each of these parameters was calculated for each cell. The nuclear diameter was measured in an arbitrary orientation for the same set of cells for which the lifetime analysis was performed. The epithelial layer thickness was measured by counting the number of image planes (10-μm z steps) between the first layer of epithelial cells and the first layer in which fibrillar collagen was

observed, or the working distance of the objective was reached.

In the stromal layer, the lifetime was averaged for the entire field of view (256×256 pixels) of one image plane containing collagen fibrils within the cheek pouch of each animal.

Changes in cellular lifetime with depth in the epithelium within an animal were evaluated by averaging all three cells within an image plane and using paired nonparametric Wilcoxon signed rank tests to compare the first and last plane in the epithelium within an animal. All cells within an animal were averaged to perform comparisons between disease states using unpaired nonparametric Wilcoxon rank-sum tests. The cellular coefficient of variation (cell standard deviation/cell mean) was calculated for each cell as a measure of intracellular variability,[32] and comparisons of all cells across disease states were made using both unpaired Wilcoxon rank-sum tests and unpaired *t* tests. Exact *p* values were computed, all *p* values are two-sided, and a *p* value of <0.05 was considered statistically significant. Parametric methods (linear mixed effects models with log-transformed outcome variables) were used for validation purposes and led to similar results. SAS version 6.12 (Cary, North Carolina) and MATLAB (The Mathworks, Inc., Natick, Massachusetts) were used for all statistical analyses.

3 Results

3.1 *Cell Culture Perturbation Studies*

Figure 1 shows multiphoton FLIM images of control cells, cells treated with $CoCl_2$, and cells treated with 3-bromopyruvate for cells plated at high density. This figure shows qualitative differences between the control and the two treated groups. $CoCl_2$ decreases the protein-bound NADH lifetime and 3-bromopyruvate increases the protein-bound NADH lifetime relative to that in the control group.

Perturbation with 3-bromopyruvate produced a statistically significant increase in the redox ratio and $CoCl_2$ produced a statistically significant decrease in the redox ratio, reflecting an alteration in the metabolism with these perturbations [Fig. 2(c), $p<0.05$]. The results for high- and low-density cells are separated because previous work has shown that the cellular lifetime of NADH depends on the cell confluency[24] (due to changes in metabolism with cell confluency). The fluorescence lifetimes at 780-nm excitation ($\tau_1=0.30\pm0.03$ ns and $\tau_2=2.40\pm0.07$ ns, averaged for control cells at low and high cell densities) are consistent with free and protein-bound NADH, respectively.[8,31] The fluorescence lifetimes at 890-nm excitation ($\tau_1=0.15\pm0.01$ ns, $\tau_2=2.44\pm0.06$ ns, $\alpha_2=17\pm2\%$, averaged for control cells at low and high cell densities) are consistent with FAD fluorescence.[33] The focus of these experiments is changes in protein-bound NADH with metabolic perturbations, so the statistical analyses of the lifetime of free NADH (τ_1) and the lifetimes of FAD are not shown. Perturbation with 3-bromopyruvate caused an increase in the fluorescence lifetime of protein-bound NADH (τ_2) and a decrease in the relative contribution of protein-bound NADH to the overall lifetime decay (α_2) in cells plated at both low and high densities [Figs. 2(a) and 2(b), $p<0.05$]. Perturbation with $CoCl_2$ caused a decrease in the fluorescence lifetime of protein-bound NADH (τ_2) and a decrease in α_2 in cells plated at low and high cell densities [Figs. 2(a) and 2(b), $p<0.05$].

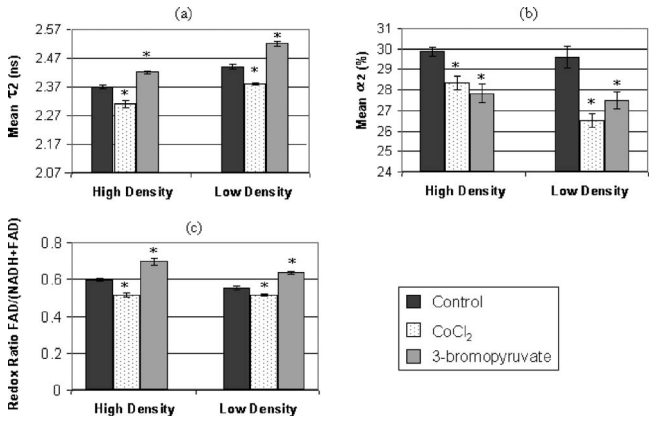

Fig. 2 NADH fluorescence lifetimes and redox ratios of MCF10A cell monolayers. Bar plots include the mean and standard error of (a) τ_2 (protein-bound NADH lifetime), (b) α_2 (percent contribution of protein-bound NADH), and (c) the redox ratio [fluorescence intensity of FAD/(NADH+FAD)] for cells plated at either high or low density. Values are plotted for control cells (high density, $n=8$; low density, $n=5$), cells treated with 3-bromopyruvate (high density, $n=6$; low density, $n=6$), which inhibits glycolysis, and cells treated with $CoCl_2$ (high density, $n=6$; low density, $n=6$), which inhibits oxidative phosphorylation. Statistically significant differences ($p<0.05$, unpaired Wilcoxon rank-sum tests) exist between control versus 3-bromopyruvate-treated and control versus $CoCl_2$-treated cells for the variables marked with an asterisk (*). The multiphoton FLIM excitation wavelength is 780 nm.

3.2 *Hamster Cheek Pouch Pathology*

Histopathology was used as the gold standard for tissue diagnosis. Of the 22 cheek pouches imaged (one per animal), 9 were diagnosed as normal (the 9 control animals), and of the 13 DMBA-treated animals 2 were diagnosed with mild dysplasia, 4 with moderate dysplasia, 4 with severe dysplasia, 2 with CIS, and 1 with SCC. For the purpose of statistical analyses, the tissue samples were divided into three categories: normal ($n=9$), low-grade precancer (mild dysplasia and moderate dysplasia, $n=6$), and high-grade precancer (severe dysplasia and CIS, $n=6$). High-grade precancers are more likely to progress to cancer than low-grade precancers.[34] The single SCC sample was not included in the statistical analysis.

3.3 *Multiphoton FLIM Images of Normal, PreCancerous, and Cancerous Tissue in Vivo*

The hamster cheek pouch has three distinct layers: an acellular superficial layer, an epithelium, and an underlying stroma. Three-dimensional image stacks of fluorescence lifetimes and the fractional contribution of the long-lifetime component of these different layers (Fig. 3) were used to determine whether multiphoton FLIM can differentiate histologically confirmed normal and dysplastic tissues.

In the normal cheek pouch [Figs. 3(a)–3(c)], the acellular superficial layer fluorescence (0 μm) has a fairly uniform distribution of long-lifetime contribution (α_2), short lifetime (τ_1), and long lifetime (τ_2). However, in low-grade [Fig. 3(d)] and high-grade precancers [Fig. 3(e)], the τ_2 of the superficial layer is nonuniform. There was no acellular superficial layer

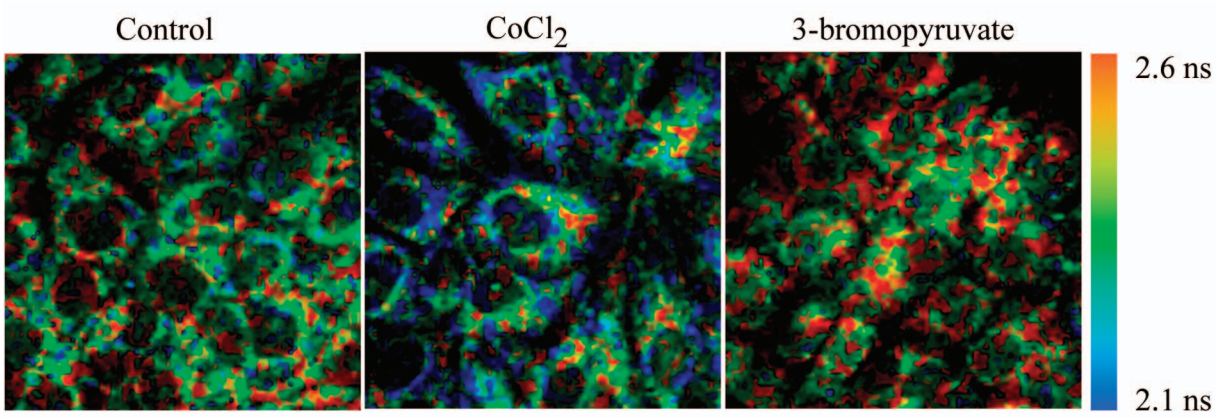

Fig. 1 Multiphoton FLIM of high-density MCF10A cells imaged in cell culture. Cells were untreated (control), treated with $CoCl_2$, or treated with 3-bromopyruvate. The color-coded value is τ_2, the protein-bound NADH lifetime (780-nm excitation).

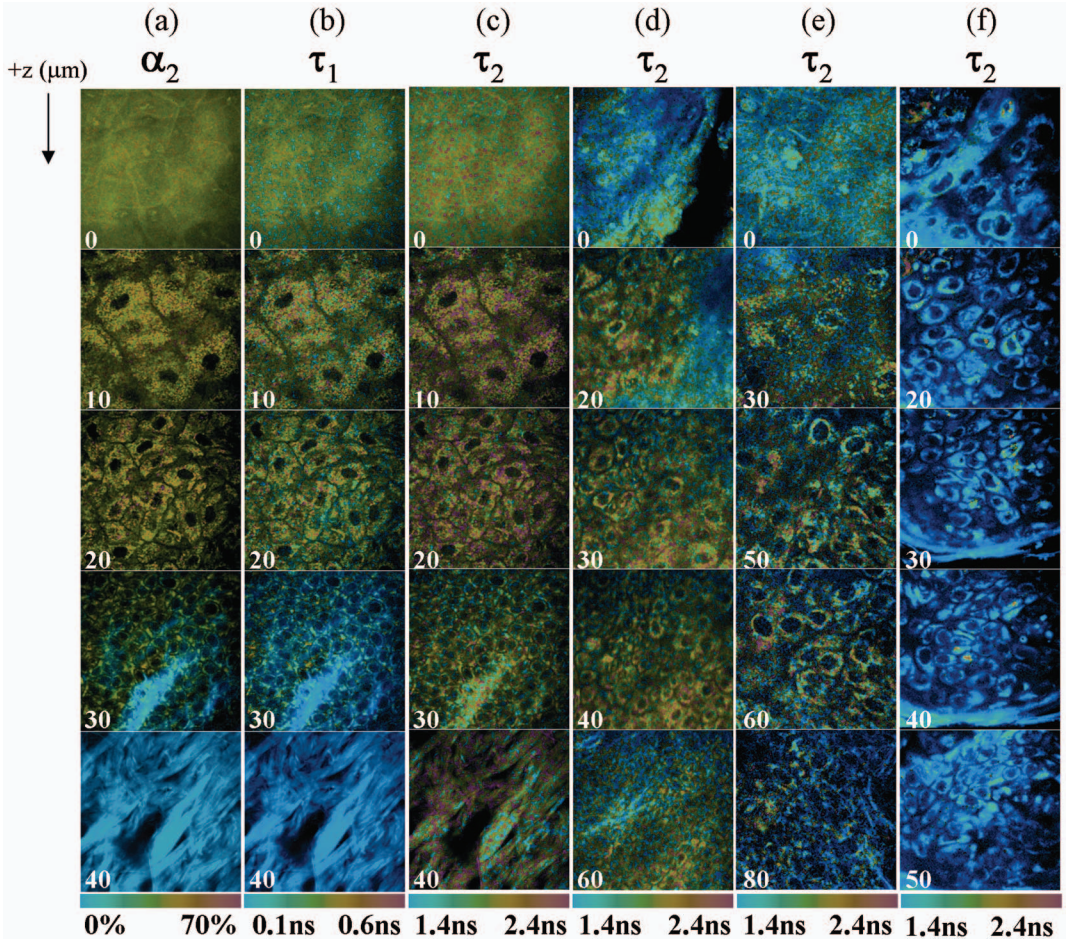

Fig. 3 Three-dimensional multiphoton FLIM images of the normal and precancerous hamster cheek pouch *in vivo*. Multiphoton FLIM of the normal hamster cheek pouch (a), (b), and (c), low-grade precancer (d, mild dysplasia), high-grade precancer (e, severe dysplasia), and SCC (f) measured *in vivo* at 780-nm excitation. Images are color coded to values of α_2 [contribution of long-lifetime component; (a)], τ_1 [short-lifetime component; (b)], and τ_2 [long-lifetime component; (c), (d), (e), and (f)]. The color bar range is at the bottom of each montage. Note that τ_1, τ_2, and α_2 each have a different color scale. The numbers in the lower left corner of each image indicate the depth below the tissue surface in micrometers, and each image is 100×100 μm.

in the one SCC sample [Fig. 3(f)]. The cytoplasmic fluorescence of the cells in the epithelium of the normal cheek pouch [Figs. 3(a)–3(c) between 10- and 30-μm depths] has a short (τ_1) and long (τ_2) lifetime component consistent with free and protein-bound NADH, respectively[8,31] (percent contribution of protein-bound NADH, α_2). The nuclear to cytoplasmic ratio of the cells increases with depth in the epithelium. However, this trend is not observed in the high-grade precancer [Fig. 3(e)] or the SCC [Fig. 3(f)]. The cellular fluorescence distribution in the high-grade precancer and SCC is also more perinuclear compared to normal tissue. The predominant lifetime component in the normal and precancerous epithelial cells is the free NADH lifetime (τ_1). The protein-bound NADH lifetime (τ_2) of precancerous and cancerous cells appears to be shorter than normal cells. The lifetime of structural proteins in the stromal layer is much different than the lifetime of NADH in the epithelial cells. In the stromal layer of the normal cheek pouch [Figs. 3(a)–3(c), 40-μm depth] τ_1 is the predominant lifetime component (the contribution of τ_2 is negligible) and its value is similar to the temporal response of the FLIM system and thus is attributed to the second-harmonic generation (SHG) of fibrillar collagen (which has a zero lifetime[35]). The stromal layer in the precancers and SCC is at a much greater depth than 40 μm.

3.4 *Statistical Analyses of Fluorescence Lifetime Parameters*

Features that were qualitatively observed to change with precancer development in the multiphoton FLIM images were next quantified to determine if these observed differences were statistically significant. First, morphological variables were quantified, and statistical tests revealed that the epithelial thickness of high-grade precancers (52 ± 19 μm) are greater than normal (18 ± 5 μm). All hamster cheek pouches were imaged to the depth of the bottom plane in the epithelium, except for one low-grade precancerous sample, in which the signal was completely attenuated before the last epithelial plane was imaged. Thus, the epithelial thickness of low-grade precancers is slightly underestimated (34 ± 19 μm) due to this one sample. Statistical tests also revealed that the nuclear diameter of low-grade (7.5 ± 0.5 μm) and high-grade (7.5 ± 0.4 μm) precancers are greater than normal (6.3 ± 0.3 μm) ($p<0.05$). More extensive analysis of morphological changes quantified from multiphoton intensity images of the DMBA-treated hamster cheek pouch at 780-nm excitation is included in a previous paper.[28]

The range of τ_1 in normal epithelial cells was 0.29 ± 0.03 ns (consistent with free NADH). The focus of this study is changes in cellular protein-bound NADH with precancer development (τ_2 in the cells), so the statistical analysis of the lifetime of free NADH is not shown.

Changes in cellular lifetime with depth in the epithelium are shown in Fig. 4. Changes in τ_2 and α_2 with depth were evaluated only within the epithelium of the hamster cheek pouch, where precancer arises. The change in lifetime with depth within the epithelium was determined from a paired comparison of the first (superficial layer) versus the last (basal layer) imaged plane of the epithelium within an animal where the greatest differences in morphology are expected. The bottom plane imaged in the epithelium of normal tissue

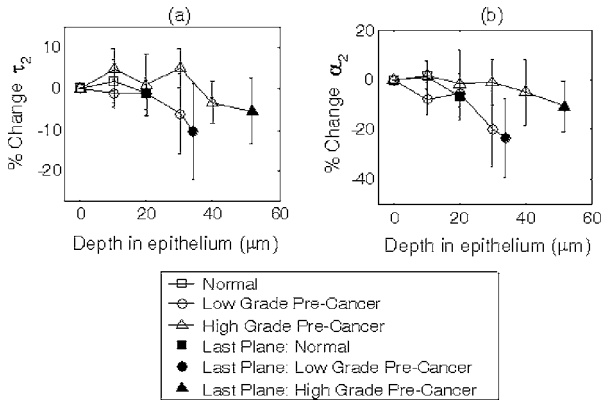

Fig. 4 Change in cellular lifetime with depth in the normal and precancerous hamster cheek pouch *in vivo*. Percent change in cellular τ_2 [protein-bound NADH lifetime; (a)] and α_2 [percent contribution of protein-bound NADH; (b)] with depth within the epithelium of the hamster cheek pouch *in vivo* measured with multiphoton FLIM at 780-nm excitation. Within each animal, τ_2 and α_2 of three cells per image plane were averaged, and then the percent changes in τ_2 and α_2 of each plane were calculated relative to those of the most superficial plane in the epithelium (defined as the first layer of cells below the acellular superficial layer). Next, the percent change in τ_2 and α_2 at each depth were averaged for all animals. Solid circles represent the mean percent change for the last plane of the epithelium for all animals, plotted at the mean depth of the last plane in the epithelium of all animals relative to the most superficial plane in the epithelium. Paired Wilcoxon signed rank tests of the first versus the last plane in the epithelium within an animal indicated a statistically significant decrease in τ_2 and α_2 with depth ($p<0.05$) in low-grade precancers.

(18 ± 2 μm) was less than that of low-grade precancers (34 ± 19 μm) and that of low-grade precancers was less than that of high-grade precancers (52 ± 19 μm). This is expected, since one of the hallmarks of epithelial precancer development is thickening of the epithelial layer with neoplasia. Paired statistical tests revealed no change in cellular τ_2 or α_2 with depth within the epithelium of normal tissues and high-grade precancers ($p>0.05$). However, cellular τ_2 and α_2 were found to decrease with depth within the epithelium of low-grade precancers ($p<0.05$). Note that the depth of the last imaged plane in the epithelium of normal tissues is much less than precancerous tissues, and thus it is not possible to compare the changes in τ_2 and α_2 over the same depth between these two tissue types.

Statistical tests also revealed that normal and dysplastic tissues are differentiated with the mean cellular protein-bound NADH lifetime (τ_2) (Table 1). The protein-bound NADH lifetime (τ_2) of both low- and high-grade precancerous cells are statistically lower than normal ($p<0.05$). The relative contribution of protein-bound NADH (α_2) for low-grade precancerous cells is also statistically lower than normal.

Intracellular variability was assessed with the cellular coefficient of variation[32] (Fig. 5). Intracellular τ_2 and α_2 variability for high- and low-grade precancers is statistically greater than normal ($p<0.05$), and intracellular α_2 variability for low-grade precancers is statistically greater than high-grade precancers ($p<0.05$).

The mean α_2 ($1.5\pm0.6\%$) and τ_1 (0.10 ± 0.003 ns) of normal and dysplastic collagen confirms that the collagen signal is 99% SHG (which has zero lifetime,[35] the minimum calcu-

Table 1 NADH fluorescence lifetimes of normal and precancerous cells in the hamster cheek pouch *in vivo*. Mean and standard deviation of cellular τ_2 (protein-bound NADH lifetime) and α_2 (percent contribution of protein-bound NADH) averaged for all cells within an animal for all normal animals ($n=9$), low-grade precancerous animals ($n=6$) and high-grade precancerous animals ($n=6$) from multiphoton FLIM at 780-nm excitation. Statistically significant differences ($p<0.05$, unpaired Wilcoxon rank-sum tests) exist between normal and low-grade precancer (*) for τ_2 and α_2, and between normal and high-grade precancer (*) for τ_2.

	τ_2 (ns)	α_2 (%)
Normal ($n=9$ animals)	2.03±0.06	37±3
Low grade ($n=6$ animals)	1.58±0.35[a]	32±4[a]
High grade ($n=6$ animals)	1.83±0.16[a]	37±4

[a]Normal versus low-grade/high-grade precancer $p<0.05$

lated lifetime constrained by the fit model is 0.1 ns).

4 Discussion

The results of this study indicate that multiphoton FLIM provides structural (cellular-level morphology in three spatial dimensions) and metabolic (NADH lifetime) information that discriminates between normal tissue and precancers *in vivo*. The morphological differences identified with precancer development (increased nuclear diameter and epithelial thickness) are consistent with a previous multiphoton microscopy study of the DMBA-treated hamster cheek pouch.[28] These morphological changes are also consistent with previous histopathology studies.[16,30,36] However, multiphoton FLIM has the advantage of resolving these structural differences *in vivo* without the need for physical sectioning, and providing functional images of tissue metabolism with the NADH fluorescence lifetime. The protein-bound NADH fluorescence lifetime discriminated normal versus high-grade and normal versus low-grade precancers *in vivo* (Table 1). The amount of protein-bound NADH relative to free NADH (α_2) also decreased with low-grade precancer compared to normal (Table 1).

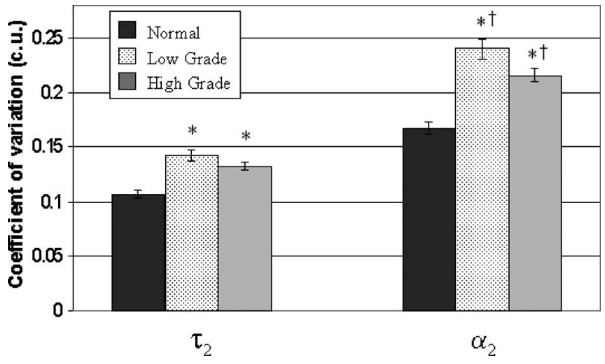

Fig. 5 Intracellular fluorescence lifetime variability of normal and precancerous cells in the hamster cheek pouch *in vivo*. Mean and standard error of the cellular coefficient of variation (cell standard deviation/cell mean) for τ_2 (protein-bound NADH lifetime) and α_2 (percent contribution of protein-bound NADH) for all normal cells ($n=81$ cells), low-grade precancerous cells ($n=72$ cells), and high-grade precancerous cells ($n=111$ cells) measured with multiphoton FLIM in the hamster cheek pouch *in vivo* at 780-nm excitation. The coefficient of variation assesses the extent of variability within a cell relative to its mean[32] (intracellular variability). Unpaired Wilcoxon rank sum tests (and *t* tests) revealed statistically significant differences ($p<0.05$) in the coefficient of variation of τ_2 and α_2 between normal cells and all precancerous cells (*), and in the coefficient of variation of α_2 between low-grade and high-grade precancerous cells (†) ($p<0.05$).

Cell culture perturbation studies (Fig. 2) revealed that the protein-bound NADH lifetime component (τ_2) increases with the addition of 3-bromopyruvate and decreases with the addition of $CoCl_2$ (consistent with previous work[24,31,37]), and these lifetime changes increase and decrease with the redox ratio, respectively. It is expected that the addition of 3-bromopyruvate causes inhibition of glycolysis, thus resulting in an increase in the redox ratio, while $CoCl_2$ causes inhibition of oxidative phosphorylation, thus decreasing the redox ratio in cell culture. Note that the results in Fig. 2 are not intended for comparison of the merits of the redox ratio versus the fluorescence lifetime. The purpose of showing the redox ratios was to use an independent method other than the fluorescence lifetime to show that there are changes in the redox state of the cells with the specific metabolic perturbations used in this study.

Changes in cellular metabolism with cancer development *in vivo* are more complex than the simple chemical perturbations to cellular metabolism in cell monolayers. Alterations in cellular metabolism with neoplasia development *in vivo* can be due to a number of factors including genetic changes, changes in tissue vascularization, and changes in metabolic demand.[6] The purpose of Fig. 2 was to show that the fluorescence lifetime is sensitive to changes in cellular metabolism in simple cell monolayers using known chemical perturbations. However, the cell monolayer results cannot be directly applied to the *in vivo* results due to the complex changes in metabolism with neoplasia development *in vivo*.

The short-lifetime component (τ_1) and long-lifetime component (τ_2) of the normal epithelial cells measured *in vivo* in the hamster cheek pouch are within the range of published values of free NADH and protein-bound NADH, respectively, in cell culture, tissue slices and *in vivo* tissue.[8,31,37–39] However, the published lifetimes of free and protein-bound NADH vary widely depending on the biological system investigated. It is also possible that FAD could contribute to the measured lifetime at a two-photon excitation wavelength of 780 nm. However, *in vivo* multiphoton fluorescence images collected at 900-nm excitation [optimal for the two-photon excitation of FAD (Ref. 26)] did not show any measurable fluorescence with our *in vivo* FLIM system, indicating that FAD is unlikely to contribute to the observed lifetime at 780-nm excitation in the hamster cheek pouch. Note that the FLIM system used for the *in vivo* experiments was not optimized for 900-nm excitation (due to low laser power and detection efficiency), but the system used for the cell culture experiments was optimized for collection at both 780 and 890 nm, so FAD fluorescence was observed in the cell culture experiments. Another source of fluorescence at this excitation wavelength is NADPH. Previous studies have shown that the concentration of NADH is about 5 times greater[40] than NADPH, the NADH quantum yield is 1.25 to 2.5 times greater[41] than NADPH, and

metabolic perturbations produce fluorescence changes dominated[42] by NADH. Thus, its likely that NADPH is responsible for a low, relatively constant fluorescence background in these studies.[37]

Normal and precancerous tissues were differentiated with the cellular protein-bound NADH lifetime (τ_2), with low- and high-grade precancerous tissues having a lower τ_2 than normal (Table 1). The Warburg effect predicts that neoplasias favor glycolysis over oxidative phosphorylation under aerobic conditions,[6,7] and given the results of the cell perturbation study (Fig. 2), the measured decrease in protein-bound NADH lifetime with neoplasia is consistent with increased levels of glycolysis. This shift to glycolysis could be due to either the Warburg effect or the Pasteur effect,[43] which is increased glycolysis due to hypoxia. Changes in the distribution of NADH enzyme binding sites associated with preferred metabolic pathways in neoplastic tissues[10] may be responsible for the change in protein-bound NADH lifetime with precancer. However, further studies are required to test this hypothesis.

Increased intracellular τ_2 and α_2 variability were observed in precancerous tissues, and low-grade precancers had increased intracellular α_2 variability compared to high-grade precancers (Fig. 5). This could be due to heterogeneous NADH binding and microenvironments within the cells. FLIM studies of precancerous cells *in vivo* at higher magnifications with perturbations to cytosolic and mitochondrial metabolism could further investigate the heterogeneity of lifetimes within individual cells.

The lifetime of low-grade precancers was found to decrease with depth in the epithelium, while the lifetime of normal and high-grade precancers did not change with depth (Fig. 4). Neoplastic cells originate near the basement membrane and can move progressively upward through the epithelium.[9] In a low-grade precancer, the epithelium is only partially occupied by the less differentiated neoplastic cells, while in a high-grade precancer, the full thickness of the epithelium is occupied by these cells.[44] It may be speculated that increased heterogeneity in cell populations in low-grade precancers may be partly responsible for the variation in lifetime with depth in these tissues.

Multiphoton FLIM is ideal for precancer detection in squamous epithelial tissues because the penetration depth of multiphoton FLIM (dependent on the optical properties of the organ site, but up to 0.3 mm in human skin,[45] for example) is comparable to the thickness of the epithelium in a variety of tissues including the cervix and oral cavity.[46] Multiphoton FLIM could also be used for other clinical applications, including noninvasive glucose monitoring in diabetics[47] and metabolic monitoring for tumor therapy. In the near term, the important findings from multiphoton FLIM studies could guide the design and development of practical time-gated fluorescence detection schemes for clinical applications. In the long term, portable technology could be engineered to enable multiphoton FLIM in a clinical setting.

Acknowledgments

The authors would like to thank John White, Axel Bergmann, and Jayne Squirrell for their scientific input, and Kristin Vrotsos and Paolo Provenzano for their help with animal and cell culture experiments, respectively. This work was supported by the National Institutes of Health (R01 EB000184) and the Department of Defense, Predoctoral Traineeship Award W81XWH-04-1-0330 (for M.S.).

References

1. K. Suhling, P. M. French, and D. Phillips, "Time-resolved fluorescence microscopy," *Photochem. Photobiol. Sci.* **4**(1), 13–22 (2005).
2. J. R. Lakowicz, *Principles of Fluorescence Spectroscopy*, Plenum Publishers, New York (1999).
3. W. Denk, J. H. Strickler, and W. W. Webb, "Two-photon laser scanning fluorescence microscopy," *Science* **248**(4951), 73–76 (1990).
4. V. E. Centonze and J. G. White, "Multiphoton excitation provides optical sections from deeper within scattering specimens than confocal imaging," *Biophys. J.* **75**(4), 2015–2024 (1998).
5. J. M. Squirrell, D. L. Wokosin, J. G. White, and B. D. Bavister, "Long-term two-photon fluorescence imaging of mammalian embryos without compromising viability," *Nat. Biotechnol.* **17**(8), 763–767 (1999).
6. C. J. Gulledge and M. W. Dewhirst, "Tumor oxygenation: a matter of supply and demand," *Anticancer Res.* **16**(2), 741–749 (1996).
7. O. Warburg, *The Metabolism of Tumors*, Constabel, London (1930).
8. J. R. Lakowicz, H. Szmacinski, K. Nowaczyk, and M. L. Johnson, "Fluorescence lifetime imaging of free and protein-bound NADH," *Proc. Natl. Acad. Sci. U.S.A.* **89**(4), 1271–1275 (1992).
9. B. Alberts, A. Johnson, J. Lewis, M. Raff, K. Roberts, and P. Walter, *Molecular Biology of the Cell*, Garland Science, New York (2002).
10. S. Banerjee and D. K. Bhatt, "Histochemical studies on the distribution of certain dehydrogenases in squamous cell carcinoma of cheek," *Indian J. Cancer* **26**(1), 21–30 (1989).
11. I. Iweibo, "Protein fluorescence and electronic energy transfer in the determination of molecular dimensions and rotational relaxation times of native and coenzyme-bound horse liver alcohol dehydrogenase," *Biochim. Biophys. Acta* **446**(1), 192–205 (1976).
12. A. R. Jones, L. Gillan, and D. Milmlow, "The anti-glycolytic activity of 3-bromopyruvate on mature boar spermatozoa in vitro," *Contraception* **52**(5), 317–320 (1995).
13. A. W. Lee and D. J. States, "Colony-stimulating factor-1 requires PI3-kinase-mediated metabolism for proliferation and survival in myeloid cells," *Cell Death Differ* **13**, 1900–1914 (2006).
14. N. S. Chandel, E. Maltepe, E. Goldwasser, C. E. Mathieu, M. C. Simon, and P. T. Schumacker, "Mitochondrial reactive oxygen species trigger hypoxia-induced transcription," *Proc. Natl. Acad. Sci. U.S.A.* **95**(20), 11715–11720 (1998).
15. E. Hervouet, P. Pecina, J. Demont, A. Vojtiskova, H. Simonnet, J. Houstek, and C. Godinot, "Inhibition of cytochrome c oxidase subunit 4 precursor processing by the hypoxia mimic cobalt chloride," *Biochem. Biophys. Res. Commun.* **344**(4), 1086–1093 (2006).
16. F. H. White, K. Gohari, and C. J. Smith, "Histological and ultrastructural morphology of 7,12 dimethylbenz(alpha)-anthracene carcinogenesis in hamster cheek pouch epithelium," *Diagn. Histopathol.* **4**(4), 307–333 (1981).
17. S. Andrejevic, J. F. Savary, C. Fontolliet, P. Monnier, and H. van Den Bergh, "7,12-dimethylbenz[a]anthracene-induced 'early' squamous cell carcinoma in the Golden Syrian hamster: evaluation of an animal model and comparison with 'early' forms of human squamous cell carcinoma in the upper aero-digestive tract," *Int. J. Exp. Pathol.* **77**(1), 7–14 (1996).
18. C. T. Chen, H. K. Chiang, S. N. Chow, C. Y. Wang, Y. S. Lee, J. C. Tsai, and C. P. Chiang, "Autofluorescence in normal and malignant human oral tissues and in DMBA-induced hamster buccal pouch carcinogenesis," *J. Oral Pathol. Med.* **27**(10), 470–474 (1998).
19. D. L. Wokosin, J. M. Squirrell, K. W. Eliceiri, and J. G. White, "An optical workstation with concurrent independent multiphoton imaging and experimental laser microbeam capabilities," *Rev. Sci. Instrum.* **74**(1), 193–201 (2003).
20. D. K. Bird, K. W. Eliceiri, C. H. Fan, and J. G. White, "Simultaneous two-photon spectral and lifetime fluorescence microscopy," *Appl. Opt.* **43**(27), 5173–5182 (2004).
21. http://www.loci.wisc.edu/WiscScan/.
22. http://www.atcc.org.
23. P. J. Keely, A. M. Fong, M. M. Zutter, and S. A. Santoro, "Alteration of collagen-dependent adhesion, motility, and morphogenesis by the expression of antisense alpha 2 integrin mRNA in mammary cells," *J. Cell. Sci.* **108**(Pt.2), 595–607 (1995).

24. D. K. Bird, L. Yan, K. M. Vrotsos, K. W. Eliceiri, E. M. Vaughan, P. J. Keely, J. G. White, and N. Ramanujam, "Metabolic mapping of MCF10A human breast cells via multiphoton fluorescence lifetime imaging of the coenzyme NADH," *Cancer Res.* **65**(19), 8766–8773 (2005).
25. B. Chance, B. Schoener, R. Oshino, F. Itshak, and Y. Nakase, "Oxidation–reduction ratio studies of mitochondria in freeze-trapped samples. NADH and flavoprotein fluorescence signals," *J. Biol. Chem.* **254**(11), 4764–4771 (1979).
26. S. Huang, A. A. Heikal, and W. W. Webb, "Two-photon fluorescence spectroscopy and microscopy of NAD(P)H and flavoprotein," *Biophys. J.* **82**(5), 2811–2825 (2002).
27. M. C. Skala, G. M. Palmer, C. Zhu, Q. Liu, K. M. Vrotsos, C. L. Marshek-Stone, A. Gendron-Fitzpatrick, and N. Ramanujam, "Investigation of fiber-optic probe designs for optical spectroscopic diagnosis of epithelial pre-cancers," *Lasers Surg. Med.* **34**(1), 25–38 (2004).
28. M. C. Skala, J. M. Squirrell, K. M. Vrotsos, J. C. Eickhoff, A. Gendron-Fitzpatrick, K. W. Eliceiri, and N. Ramanujam, "Multiphoton microscopy of endogenous fluorescence differentiates normal, precancerous, and cancerous squamous epithelial tissues," *Cancer Res.* **65**(4), 1180–1186 (2005).
29. A. Schonle, M. Glatz, and S. W. Hell, "Four-dimensional multiphoton microscopy with time-correlated single-photon counting," *Appl. Opt.* **39**(34), 6306–6311 (2000).
30. D. G. MacDonald and S. M. Saka, *Structural Indicators of the High Risk Lesion*, Cambridge Univ. Press, Cambridge (1991).
31. H. Schneckenburger, M. Wagner, P. Weber, W. S. L. Strauss, and R. Sailer, "Autofluorescence lifetime imaging of cultivated cells using a UV picosecond laser diode," *J. Fluoresc.* **14**, 649–654 (2004).
32. J. Gibbons and S. Chakraborti, *Nonparametric Statistical Inference*, Marcel Dekker, New York (1992).
33. F. Tanaka, N. Tamai, and I. Yamazaki, "Picosecond-resolved fluorescence spectra of D-amino-acid oxidase. A new fluorescent species of the coenzyme," *Biochemistry* **28**(10), 4259–4262 (1989).
34. G. F. Sawaya, A. D. Brown, A. E. Washington, and A. M. Garber, "Clinical practice. Current approaches to cervical-cancer screening," *N. Engl. J. Med.* **344**(21), 1603–1607 (2001).
35. P. J. Campagnola and L. M. Loew, "Second-harmonic imaging microscopy for visualizing biomolecular arrays in cells, tissues and organisms," *Nat. Biotechnol.* **21**(11), 1356–1360 (2003).
36. Y. V. Xiang, "Quantitative study on esophageal cytology. I. Quantitative morphologic studies of normal, dysplastic and malignant squamous cells," *Zhonghua Zhong Liu Za Zhi* **12**(2), 92–94 (1990).
37. H. D. Vishwasrao, A. A. Heikal, K. A. Kasischke, and W. W. Webb, "Conformational dependence of intracellular NADH on metabolic state revealed by associated fluorescence anisotrophy," *J. Biol. Chem.* **280**, 25119–25126 (2005).
38. R. Niesner, B. Peker, P. Schlusche, and K. H. Gericke, "Noniterative biexponential fluorescence lifetime imaging in the investigation of cellular metabolism by means of NAD(P)H autofluorescence," *ChemPhysChem* **5**(8), 1141–1149 (2004).
39. K. König and I. Riemann, "High-resolution multiphoton tomography of human skin with subcellular spatial resolution and picosecond time resolution," *J. Biomed. Opt.* **8**(3), 432–439 (2003).
40. L. K. Klaidman, A. C. Leung, and J. D. Adams, Jr., "High-performance liquid chromatography analysis of oxidized and reduced pyridine dinucleotides in specific brain regions," *Anal. Biochem.* **228**(2), 312–317 (1995).
41. Y. Avi-Dor, J. Olson, M. Doherty, and N. Kaplan, "Fluorescence of pyridine nucleotides in mitochondria," *J. Biol. Chem.* **237**(7), 2377–2383 (1962).
42. B. Chance, J. Williamson, D. Jamieson, and B. Schoener, "Properties and kinetics of reduced pyridine nucleotide fluorescence of the isolated and in vivo rat heart," *Biochem. Z.* **341**, 357–377 (1965).
43. T. Schroeder, H. Yuan, B. L. Viglianti, C. Peltz, S. Asopa, Z. Vujaskovic, and M. W. Dewhirst, "Spatial heterogeneity and oxygen dependence of glucose consumption in R3230Ac and fibrosarcomas of the Fischer 344 rat," *Cancer Res.* **65**(12), 5163–5171 (2005).
44. I. Pavlova, K. Sokolov, R. Drezek, A. Malpica, M. Follen, and R. Richards-Kortum, "Microanatomical and biochemical origins of normal and precancerous cervical autofluorescence using laser-scanning fluorescence confocal microscopy," *Photochem. Photobiol.* **77**(5), 550–555 (2003).
45. P. T. So, C. Y. Dong, B. R. Masters, and K. M. Berland, "Two-photon excitation fluorescence microscopy," *Annu. Rev. Biomed. Eng.* **2**, 399–429 (2000).
46. D. H. Cormack, *Clinically Integrated Histology*, Lipincott-Rave, Philadelphia (1998).
47. N. D. Evans, L. Gnudi, O. J. Rolinski, D. J. Birch, and J. C. Pickup, "Glucose-dependent changes in NAD(P)H-related fluorescence lifetime of adipocytes and fibroblasts in vitro: potential for non-invasive glucose sensing in diabetes mellitus," *J. Photochem. Photobiol., B* **80**(2), 122–129 (2005).